Published in final edited form as:

Chem Commun (Camb). 2021 February 18; 57(14): 1770–1773. doi:10.1039/d0cc06400a.

Magnetic resonance thermometry using a Gd^{III}-based contrast agent

S. A. Amali S. Subasinghe[a], **Jonathan Romero**[b], **Cassandra L. Ward**[c], **Matthew D. Bailey**[a], **Donna R. Zehner**[b], **Prakrut J. Mehta**[b], **Fabio Carniato**[d], **Mauro Botta**[d], **Jason T. Yustein**[e], **Robia G. Pautler**[b], **Matthew J. Allen**[a]

[a]Department of Chemistry, Wayne State University, 5101 Cass Avenue, Detroit, Michigan 48202, United States

[b]Department of Molecular Physiology and Biophysics, Baylor College of Medicine, Houston, Texas 77030, United States

[c]Lumigen Instrument Center, Wayne State University, 5101 Cass Avenue, Detroit, Michigan 48202, United States

[d]Dipartimento di Scienze e Innovazione Tecnologica, Università del Piemonte Orientale “Amedeo Avogadro”, Viale T. Michel 11, 15121 Alessandria, Italy

[e]Integrative Molecular and Biomedical Sciences and the Department of Pediatrics in the Texas Children’s Cancer and Hematology Centers and The Faris D. Virani Ewing Sarcoma Center, Baylor College of Medicine, Houston, Texas 77030, United States

Abstract

The complexes described here serve as contrast agents for magnetic resonance imaging thermometry. The complexes differentially enhance contrast between 275 and 325 K. The basis of the temperature response of the fluorinated contrast complex is the modulation of water exchange caused by trifluoromethyl groups that can be chemically controlled.

Graphical Abstract

Electronic Supplementary Information (ESI) available: Experimental procedures, synthesis and characterization, crystallographic data, thermal gravimetric analysis data, luminescence-decay measurements, ANOVA test results, parameters from the analysis of NMRD and variable-temperature NMR data, and plots of T_{1M} and τ_M as a function of temperature at 9.4 T (.pdf file). CCDC 1991782 and 1991783. For ESI and crystallographic data in CIF or other electronic format see DOI: 10.1039/x0xx00000x

Conflicts of interest

There are no conflicts to declare.

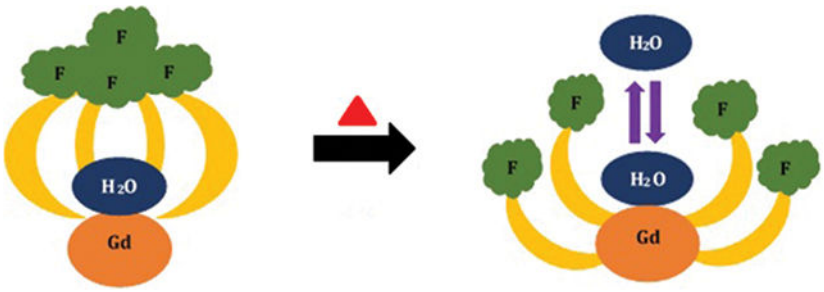

Thermal therapies have gained interest in recent years as treatments for diseases.[1–4] This interest has driven efforts focusing on the measurement of temperatures in living organisms using various methods, including thermocouples,[5] microneedle array electrodes,[6] paramagnetic thermosensitive liposomes,[7,8] spin transition molecular materials,[9–11] and paramagnetic lanthanide complexes as contrast agents for imaging.[12–14] Many of these methods are invasive or use contrast agents that report temperature as a step function instead of reporting a range of temperatures. However, thermometry using magnetic resonance imaging (MRI) is a promising technique for use with thermal therapies to accurately monitor heterogeneously distributed temperatures in living organisms.[15–17] Because MRI-based monitoring of thermal therapies is noninvasive, it is possible to map temperature in real-time. The combination of MRI with temperature-responsive contrast agents can increase the ability to report temperature. For example, lanthanide-based contrast agents for MRI have been encapsulated in macromolecular hydrogel systems or liposomes to increase contrast enhancement from dark to bright upon increasing temperature;[18–20] however, there is a lack of small-molecule MRI thermometers that transition from dark to bright with increasing temperature. Here, we present a Gd^{III}-containing complex that displays a decrease in contrast enhancement and its fluorinated Gd^{III}-containing complex that increases innersphere relaxivity with increasing temperature over a biologically relevant range.

We drew inspiration from a redox-responsive fluorous Eu^{II}-containing complex that displayed temperature-dependent relaxivity.[21] We hypothesized that replacing Eu^{II} with Gd^{III} would isolate temperature control from redox activity if the coordination chemistry remained similar. To test this hypothesis, we synthesized Gd^{III}-containing complex **1** that contained 12 chemically equivalent fluorine atoms (Fig. 1). A methylated analog of the Gd^{III}-containing complex, **2**, was also synthesized to investigate the structural changes that make this fluorinated complex temperature sensitive. Both complexes were characterized for identity and purity using high-resolution mass spectrometry and elemental analysis.

Having characterized complexes **1** and **2**, we investigated whether structures of the fluorous complex and the methyl analog were the same. The crystal structure of fluorous complex **1** has a cage-like structure formed by the fluorinated arms of the complex (Fig. 1). The uncommon cage-like structure encapsulates a molecule of water that is coordinated to Gd^{III}, like the structure of the divalent europium analog.[21] Methylated analog **2** does not share the cage-like structure. A coordinated molecule of water is present in **2**, but the arms of **2** extend away from the Gd^{III} ion. The orientation of the arms of a tetraamide lanthanide complex extending away from the metal is consistent with observations of almost all other lanthanide-

containing tetraamide complexes.[22–24] These observations demonstrate that two otherwise similar Gd^{III}-containing complexes differ in their structure due to fluorous interactions.[25,26]

To learn how these complexes behave in solution, we measured the relaxivities of **1** and **2** as a function of temperature (Fig. 2). We selected a broad temperature range, which included ambient temperature and body temperature, to obtain accurate fitting curves. For **1**, relaxivity remained constant at 1.9 mM^{-1} s^{-1} from 293 to 318 K at 9.4 T (ANOVA data available in the ESI), with an increase in innersphere relaxivity over the same range at both 1.4 and 9.4 T (Fig. 2). Further, we observed a steady decrease in the relaxivity, both observed and innersphere, of **2** with increasing temperature. The decrease in relaxivity observed with **2** over the temperature range studied is consistent with other complexes of Gd^{III} including clinically approved contrast agents and tetraamide complexes.[27–29] The similar relaxivity of **2** with other complexes coupled with the similarity in molecular weight (58 Dalton difference) and structure (same types and numbers of donors on the ligands) between **1** and **2** make the opposite influence of temperature on innersphere relaxivity between the complexes unique. As exemplified by other Gd^{III}-containing complexes studied over similar temperature ranges,[27–29] relaxivity is expected to decrease with increasing temperature, like we observed with **2**, because of the increased tumbling rates of molecules associated with higher temperatures. The temperature-independent behavior observed with **1**, despite having a similar molecular weight to **2**, indicates a different driving force for the observed change caused by minor changes to the periphery of the ligand. Based on Solomon– Bloembergen–Morgan theory,[30] a change in the number of coordinated water molecules that are in exchange with bulk water could cause the observed change in relaxivity.

Suspecting that the temperature-dependent innersphere relaxivity of **1** was due to a change in the number of water molecules that were both coordinated and exchanging with bulk water, we used luminescence spectroscopy to determine the water-coordination numbers of **1** and **2** at 288, 298, and 313 K. In these studies, Eu^{III} is often used as a luminescent surrogate for Gd^{III}, therefore, we synthesized the Eu^{III}-containing analogs of **1** and **2**. We performed luminescence-decay measurements of the Eu^{III} analogs of **1** and **2** in H_2O and D_2O (data available in the ESI) and determined water-coordination number using the Horrocks equation.[31] We determined the water-coordination number to be 0.9 for both **1** and **2** at all three temperatures; implying that both **1** and **2** contain one coordinated water molecule in solution across the entire temperature range of our studies. This observation is consistent with the solid-state structures of **1** and **2**. Although there was no difference in the number of coordinated water molecules between **1** and **2** in solution, those coordinated water molecules only have a substantial influence on relaxivity if they are in fast exchange with bulk water. We suspected that if the cage of CF_3 groups surrounding the coordinated water molecule of **1** inhibited water exchange in a temperature-dependent fashion, then the inhibition could be the driving force behind our observed change in relaxivity.

To test this hypothesis, we evaluated molecular parameters that determine relaxivity using variable-field (0.01 to 120 MHz) ^1H nuclear magnetic relaxation dispersion analysis (NMRD) of complexes **1** and **2** (Fig. 3). NMRD analysis enabled us to fit data to theoretical models of paramagnetic relaxation and extract parameters that govern the relaxivity. Data for

NMRD profiles were acquired at 298, 308, and 318 K and fitted using Solomon–Bloembergen–Morgan theory of innersphere paramagnetic relaxivity in conjunction with Freed theory for outer-sphere contribution. Water-coordination number (q), Gd^{III}–water proton distance (r), distance of closest approach of outer-sphere water (a), diffusion coefficient (D), and the activation energy of the electronic correlation time for the modulation of the zero-field splitting interaction (E_v) were set to fixed standard values.[30,32] All the other parameters were obtained using least square fitting method (Table 1 and Table S4). The NMRD profiles of **1** and **2** showed that relaxivity of **2** was greater than **1** at every field studied, and the relaxivities of **1** and **2** are largest at low field strengths (<1 MHz). The NMRD profiles are characterized by the typical shape of low molecular weight Gd^{III}-containing chelates,[33] featuring a plateau at field strengths below 0.1 MHz and a dispersion between 2 and 8 MHz. At field strengths of 10 MHz and larger, the innersphere relaxivities of **1** and **2** are dominated by rotational dynamics that are described in terms of a rotational correlation time τ_R (equation S3). However, the amplitude of the profiles of **1** and **2** are significantly different, and this difference is attributable to a different contribution of the innersphere mechanism in the two cases: large for **2** and significantly small for **1**. In fact, the calculated water-exchange rate of **1** is an order of magnitude slower than the water-exchange rate of **2** over the entire temperature range that we studied. Other than the τ_m values of **1** and **2**, which are 80× different from each other, there is almost no change in the other parameters between the two molecules. The one exception is a slight difference in τ_R that is largely due to the imprecision associated with this term for molecules with extremely slow water-exchange rates (small innersphere contribution).

$$r_1 = \frac{c}{55.5(T_{1m} + \tau_m)} \quad \text{Eq 1}$$

Based on the molecular parameters of **1** and **2**, we calculated the longitudinal proton relaxation time (T_{1m}) and residence lifetime of bound water molecules (τ_m) of **1** and **2** at 1.4 and 9.4 T (Fig. 4 and Fig. S8). The values of T_{1m} were similar to each other for both **1** and **2**, which is not surprising because in both molecules water is coordinated to Gd^{III} in similar coordination environments. The value of τ_m, however, was 80 times larger for **1** than with **2**. That difference lead to $T_{1m} \approx \tau_m$ (slow/intermediate-exchange regime) for **1**, and $\tau_m < T_{1m}$ (fast-exchange regime) for **2** across the entire temperature range that we studied. Because innersphere proton relaxivity is inversely proportional to T_{1m} and τ_m (equation 1, where c is the molal concentration of Gd and there is a water-coordination number of one), the term that dominates the value in equation 1 limits relaxivity. With **2**, T_{1m} dominates τ_m and, therefore, limits relaxivity. The value of T_{1m} for **2** slightly increases (0.189 to 0.207 ms at 1.4 T) with increasing temperatures (280 to 315 K) because of the decrease of rotational correlation times due to rapid molecular rotations. We observed a small and steady decrease in the relaxivity of **2** due to shortening of τ_R with increasing temperature. However, τ_m contributes to the relaxivity of **1**, and therefore, observably governs the relaxivity of **1**. Because τ_m decreases [water-exchange rate ($k_{ex} = 1/\tau_m$) increases] with increasing temperature, the innersphere relaxivity of **1** increased with increasing temperature (Fig. 2). In this case, the decrease in τ_m makes the contribution of T_{1m} and, therefore, of the innersphere mechanism gradually more relevant. This increase in innersphere relaxivity with

1 is enough to negate the increase molecular motions at higher temperatures, leading to a temperature-independent observed relaxivity. The good correspondence between the calculated and experimental values supports the accuracy of the analysis.

The different water-exchange modulation of **1** compared to **2** is likely due to its unusual conformation brought about by the 12 F atoms. At colder temperatures, the encapsulated innersphere water molecule in the cage-like structure restricts water exchange between the coordinated water trapped in the cage and bulk water. At warmer temperatures, molecular motions of the fluorinated arms increase access to the coordinated water molecule to increase the water-exchange rate, consistent with an increase in innersphere relaxivity. Usually, the relaxivity of small-molecule contrast agents is largely influenced by water-coordination number and rotational correlation time.[30] Lanthanide-containing complexes are sometimes conjugated with macromolecules including proteins to slow rotation to the point that water residence lifetime influences relaxivity.[30] In the system described here that does not involve conjugation with macromolecules, the relaxivity of **1** is modulated by water residence lifetime as a function of temperature. This conformational-change-driven modulation of water exchange is unique to our system and different from other lanthanide-containing tetraamide complexes.[22–24]

In conclusion, we have synthesized Gd^{III}-containing complexes for MRI thermometry. The nonfluorinated agent, **2**, decreases observed relaxivity with increasing temperature between ambient and body temperature, and the fluorinated agent, **1**, displays in increase in innersphere relaxivity over that same range, which is a critical step toward dark-to-bright contrast agents. These changes are an effect of a small change from CH_3 to CF_3 on the periphery of the complex with nearly identical coordination environments. While the CF_3 complex is not optimized as a preclinical agent for thermometry, the two complexes provide a foundation for the ability to prepare thermometers using changes to ligand periphery: we expect these results, in combination with methods to limit the influence of molecular motions and concentration,[34] to advance the study of temperature in vivo in a wide variety of systems and in association with thermal therapies.

Supplementary Material

Refer to Web version on PubMed Central for supplementary material.

Acknowledgments

The authors acknowledge the National Institutes of Health (R01EB026453) for financial support. We thank Charles Winter for the use of the thermal gravimetric analyzer and Federico Rabuffetti and Dinesh Amarasinghe for the use of the spectrofluorometer.

References

1. Long D, Liu T, Tan L, Shi H, Liang P, Tang S, Wu Q, Yu J, Dou J and Meng X, ACS Nano, 2016, 10, 9516. [PubMed: 27689440]
2. Long D, Mao J, Liu T, Fu C, Tan L, Ren X, Shi H, Su H, Ren J and Meng X, Nanoscale, 2016, 8, 11044. [PubMed: 27174624]
3. Ge X, Song Z-M, Sun L, Yang Y-F, Shi L, Si R, Ren W, Qiu X and Wang H, Biomaterials, 2016, 108, 35. [PubMed: 27619238]

4. Fu C, Zhou H, Tan L, Huang Z, Wu Q, Ren X, Ren J and Meng X, ACS Nano, 2018, 12, 2201. [PubMed: 29286623]
5. Orenstein A, Kostenich G, Tsur H, Kogan L and Malik Z, Cancer Lett, 1995, 93, 227. [PubMed: 7621433]
6. Sun Y, Ren L, Jiang L, Tang Y and Liu B, Sensors, 2018, 18, 1193.
7. Tagami T, Foltz WD, Ernsting MJ, Lee CM, Tannock IF, May JP and Li S-D, Biomaterials, 2011, 32, 6570. [PubMed: 21641639]
8. Kuijten MMP, Degeling MH, Chen JW, Wojtkiewicz G, Waterman P, Weissleder R, Azzi J, Nicolay K and Tannous BA, Sci. Rep, 2015, 5, 17220. [PubMed: 26610702]
9. Muller RN, Vander Elst L and Laurent S, J. Am. Chem. Soc, 2003, 125, 8405. [PubMed: 12837114]
10. Jeon IR, Park JG, Haney CR and Harris TD, Chem. Sci, 2014, 5, 2491.
11. Thorarinsdottir AE, Gaudette AI and Harris TD, Chem. Sci, 2017, 8, 2448. [PubMed: 28694955]
12. Zhang S, Malloy CR and Sherry AD, J. Am. Chem. Soc, 2005, 127, 17572. [PubMed: 16351064]
13. Delli Castelli D, Terreno E and Aime S, Angew. Chem. Int. Ed, 2011, 50, 1798.
14. Finney K-LNA, Harnden AC, Rogers NJ, Senanayake PK, Blamire AM, O'Hogain D and Parker D, Chem. Eur. J, 2017, 23, 7976. [PubMed: 28378890]
15. Cheng C-A, Chen W, Zhang L, Wu HH and Zink JI, J. Am. Chem. Soc, 2019, 141, 17670. [PubMed: 31604010]
16. Piraner DI, Abedi MH, Moser BA, Lee-Gosselin A and Shapiro MG, Nat. Chem. Biol, 2017, 13, 75. [PubMed: 27842069]
17. Du Q, Ma T, Fu C, Liu T, Huang Z, Ren J, Shao H, Xu K, Tang F and Meng X, ACS Appl. Mater. Interfaces, 2015, 7, 13612. [PubMed: 26031508]
18. Shuhendler AJ, Staruch R, Oakden W, Gordijo CR, Rauth AM, Stanisz GJ, Chopra R and Wu XY, J. Control. Release, 2012, 157, 478. [PubMed: 21939700]
19. Peller M, Schwerdt A, Hossann M, Reinl HM, Wang T, Sourbron S, Ogris M and Lindner LH, Invest. Radiol 2008, 43, 877. [PubMed: 19002060]
20. Tashjian JA, Dewhirst MW, Needham D and Viglianti BL, Int. J. Hyperthermia, 2008, 24, 79. [PubMed: 18214771]
21. Basal LA, Bailey MD, Romero J, Ali MM, Kurenbekova L, Yustein J, Pautler RG and Allen MJ, Chem. Sci, 2017, 8, 8345. [PubMed: 29780447]
22. Dickins RS, Howard JAK, Lehmann CW, Moloney J, Parker D and Peacock RD, Angew. Chem. Int. Ed. Engl, 1997, 36, 521.
23. Srivastava K, Weitz EA, Peterson KL, Marjańska M and Pierre VC, Inorg. Chem, 2017, 56, 1546. [PubMed: 28094930]
24. Thompson AL, Parker D, Fulton DA, Howard JAK, Pandya SU, Puschmann H, Senanayake K, Stenson PA, Badari A, Botta M, Avedano S and Aime S, Dalton Trans, 2006, 47, 5605.
25. Omorodion H, Twamley B, Platts JA and Baker RJ, Cryst. Growth Des, 2015, 15, 2835.
26. Li B-Y, Juang DS, Adak AK, Hwang K-C and Lin C-C, Sci. Rep, 2017, 7, 7053. [PubMed: 28765646]
27. Kálmán FK, Woods M, Caravan P, Jurek P, Spiller M, Tircsó G, Király R, Brücher E and Sherry AD, Inorg. Chem, 2007, 46, 5260. [PubMed: 17539632]
28. Zhang S, Wu K, Biewer MC and Sherry AD, Inorg. Chem 2001, 40, 4284. [PubMed: 11487334]
29. Laurent S, Vander Elst L and Muller RN, Contrast Med. Mol. Imaging, 2006, 1, 128.
30. Helm L, Morrow JR, Bond CJ, Carniato F, Botta M, Braun M, Baranyai Z, Pujales-Paradela R, Regueiro-Figueroa M, Esteban-Gómez D, Platas-Iglesias C and Scholl TJ in Contrast Agents for MRI: Experimental Methods (Eds.: Pierre VC and Allen MJ), Royal Society of Chemistry, 2018, pp. 121–242.
31. Supkowski RM and Horrocks WD Jr., Inorg. Chim. Acta, 2002, 340, 44.
32. Aime S, Botta M, Esteban-Gómez D and Platas-Iglesias C, Mol. Phys, 2019, 117, 898.
33. Caravan P, Chem. Soc. Rev, 2006, 35, 512. [PubMed: 16729145]
34. Ekanger LA and Allen MJ, Metallomics, 2015, 7, 405. [PubMed: 25579206]

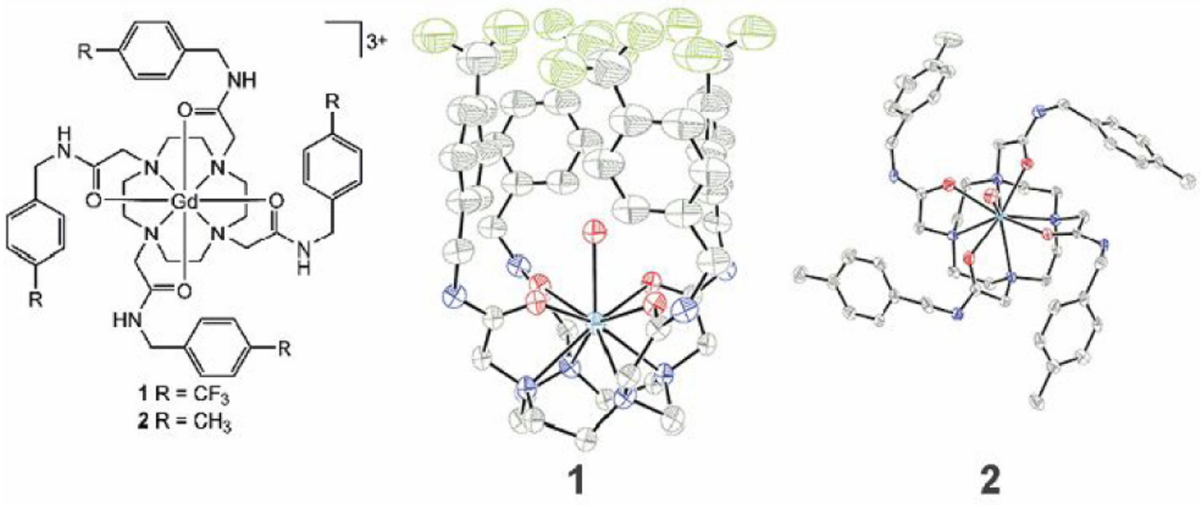

Fig. 1.

Chemical (left) and crystallographic structures from diffraction of Gd^{III}-containing complexes **1** (center) and **2** (right). Thermal ellipsoids are drawn at 50% probability. Counterions, outer-sphere water molecules, and hydrogen atoms are not shown for clarity. Grey = carbon; blue = nitrogen; red = oxygen; green = fluorine; and sea green = gadolinium. Crystallographic data for the structures has been deposited at the Cambridge Crystallographic Data Centre under deposition numbers CCDC 1991782 and 1991783.

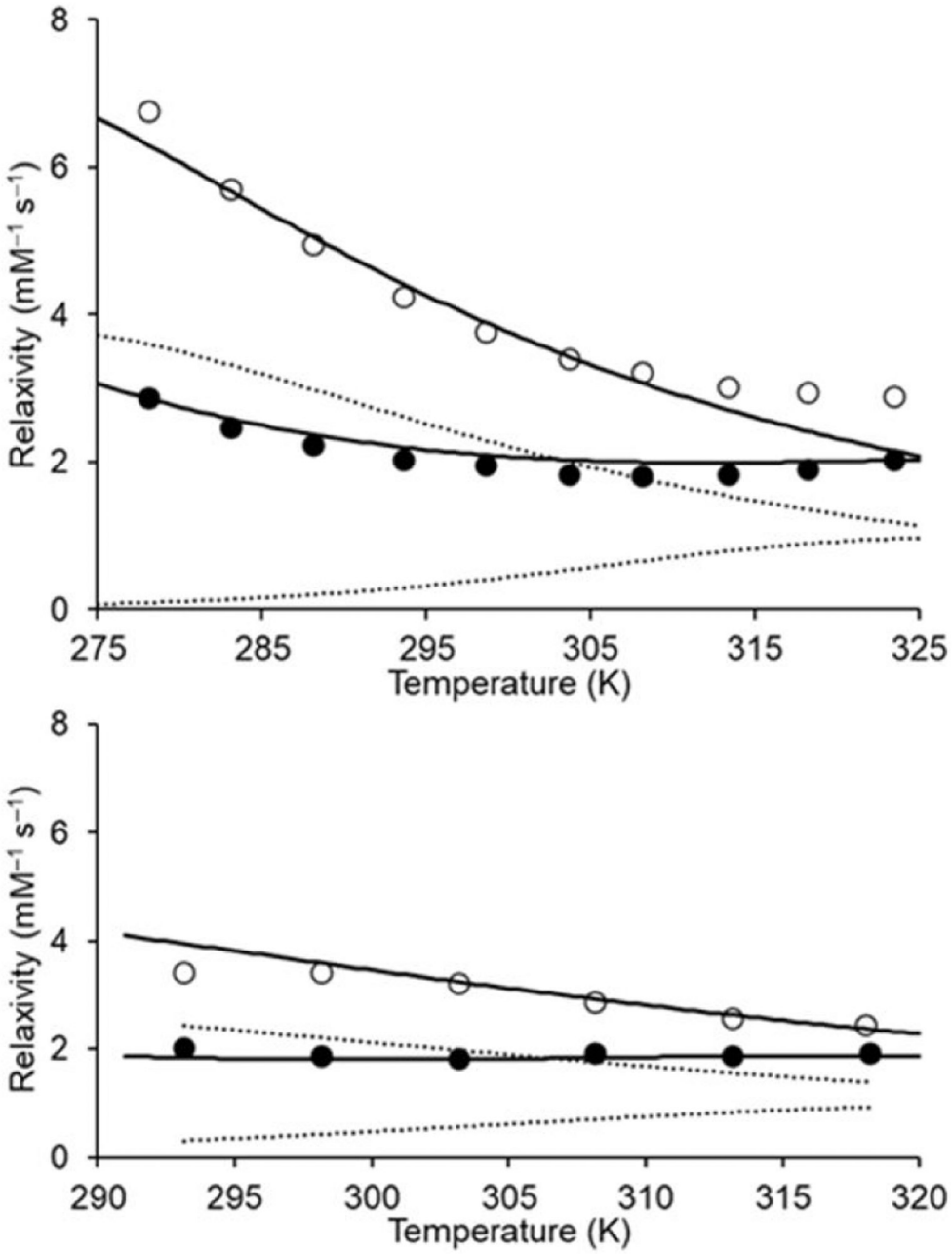

Fig. 2.

Plots of relaxivity vs temperature at (top) 1.4 and (bottom) 9.4 T. Solutions of **1** (●) and **2** (○) used for relaxivity measurements were prepared in aqueous 3-morpholinopropane-1-sulfonic acid buffer (pH 7.4). The solid and dashed lines, representing total and innersphere relaxivity, respectively, were calculated using NMRD best-fit parameters (Table S4).

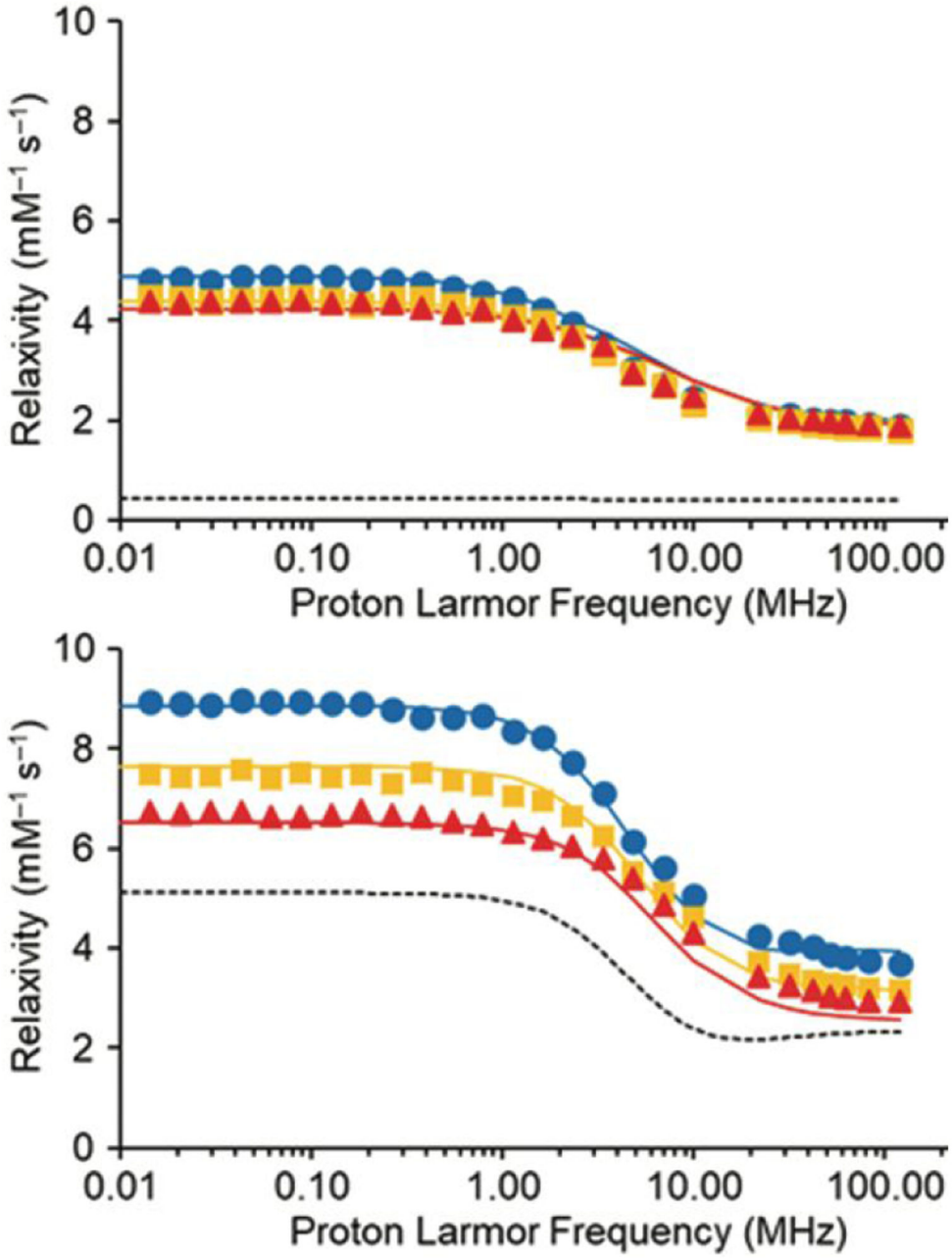

Fig. 3.

NMRD profiles of solutions of (top) **1** and (bottom) **2** in aqueous 3-morpholinopropane-1-sulfonic acid buffer (pH 7.4) at 298 (●), 308 (■), and 318 (▲) K. Solid and dashed lines, representing total and innersphere relaxivity, respectively, were fitted assuming $r = 3.1$ Å, $q = 1$, $a = 4.3$ Å, and $^{298}D = 2.24 \times 10^5$ cm^2 s^{-1}.

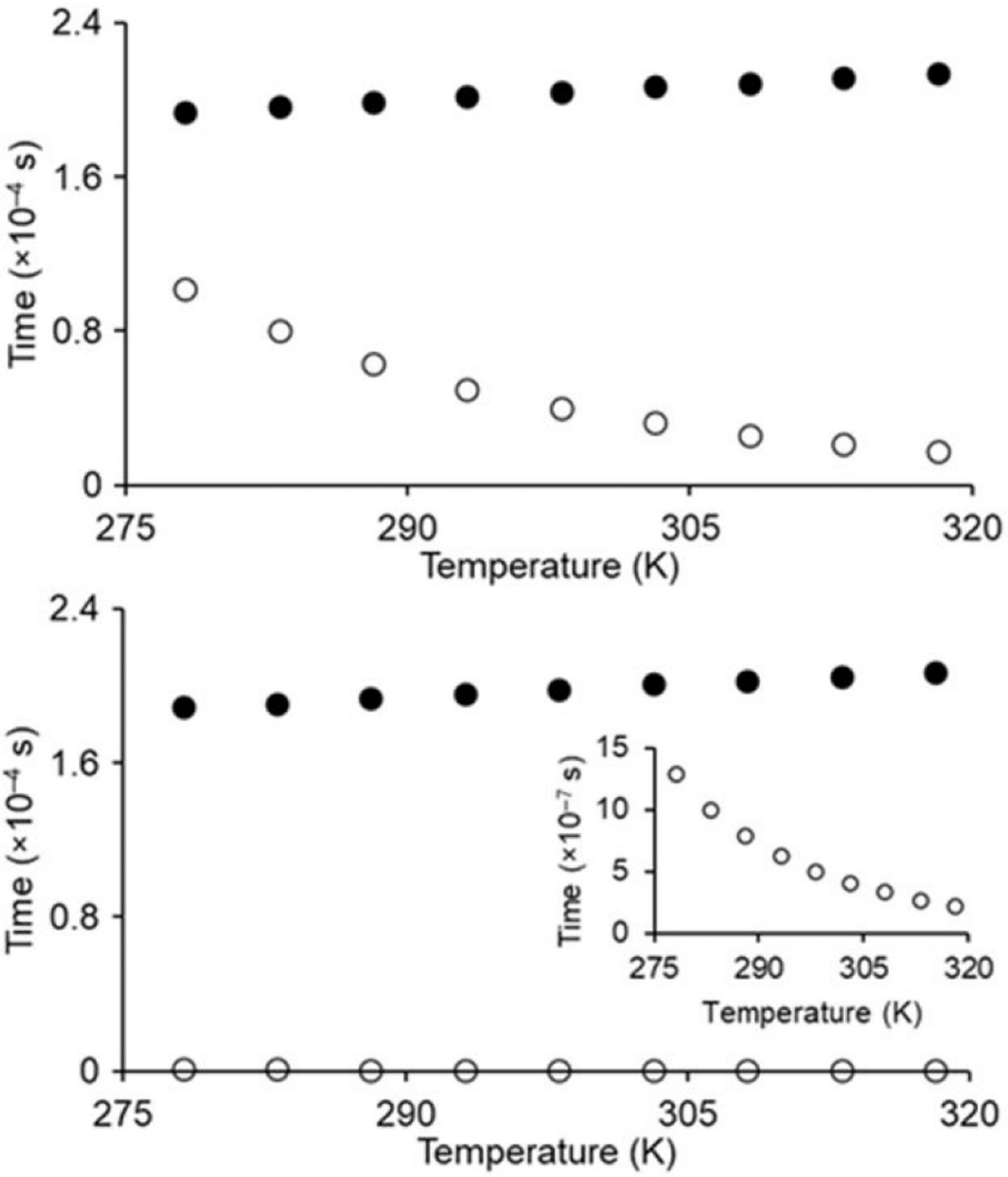

Fig. 4.

Plots of T_{1m} (●) and τ_m (○) of **1** (top graph) and **2** (bottom graph) as a function of temperature at 1.4 T. The inset on the bottom plot shows the behavior of τ_m for **2**.

Table 1

Selected parameters obtained from the fitting of the NMRD profiles of **1** and **2**.

Parameters	1	2
Δ^2 (10^{19} s^{-2})	3.0 ± 0.2	5.3 ± 0.3
τ_v (ps)	6±1	8±1
τ_R (ps)	100 ± 5	81 ± 2
ΔH_m (kJ mol^{-1})	52 ± 3	30 ± 3
τ_m (μs)	40 ±1	0.5 ±0.1